



Semi-analytical Approach to Modeling Forchheimer Flow in Porous Media at Meso- and Macroscales

A. B. Zolotukhin¹ · A. T. Gayubov¹

Received: 18 March 2020 / Accepted: 1 December 2020 / Published online: 30 January 2021
© The Author(s), under exclusive licence to Springer Nature B.V. part of Springer Nature 2021

Abstract

Darcy's law (which states that a fluid flow rate is directly proportional to the pressure gradient) is shown to be accurate in a rather narrow range of flow velocities. Numerous studies show that at low pressure gradients gas slippage effect occurs, which gives overestimated flow rates compared to Darcy's law. At higher flow rates, Darcy's law is usually replaced by the Forchheimer equation which accounts for inertial forces including a quadratic term in the flow rate. Darcy's and Forchheimer's laws and the problem of detecting transitions between their ranges of applicability are discussed in this study. Analysis of experimental data shows that deviation from Darcy's law is governed by the Forchheimer number, which is defined by the authors as a product of tortuosity and Reynolds number. The use of the Forchheimer number and semi-analytical approaches enables us to describe non-Darcy flow as a simple universal equation valid for any flow geometry. Comparison of the experimental data with predictions based on a semi-analytical model shows excellent agreement for a wide range of reservoir properties.

Keywords Forchheimer's law · Non-Darcy coefficient · Reynolds number · Forchheimer number · Tortuosity · Permeability · Porosity

List of Symbols

D_p	Particles diameter, m
D_t	Throat diameter, m
E	Non-Darcy effect
F	Formation resistivity factor
Fo	Forchheimer number
Fo_D	Forchheimer number related to Darcy flow conditions
Fo_c	Critical Forchheimer number
$Fo_{c\text{exp}}$	Experimentally measured critical Forchheimer number
$Fo_{c\text{sim}}$	Critical Forchheimer number obtained during the simulation

✉ A. B. Zolotukhin
anatoly.zolotukhin@gmail.com

A. T. Gayubov
a.t.gayubov@gmail.com

¹ Department of Oil and Gas Field Development, Gubkin Russian State University of Oil and Gas (National Research University), Moscow, Russia

P	Pressure, Pa
P_0	Standard pressure, Pa
P_1	Inlet pressure, Pa
P_2	Outlet pressure, Pa
P_D	Pressure related to Darcy flow conditions, Pa
P_F	Pressure related to Forchheimer flow conditions, Pa
P_e	External boundary pressure, Pa
P_w	Bottomhole pressure, Pa
Re	Reynolds number
Re_D	Reynolds number related to Darcy flow conditions
Re_F	Reynolds number related to Forchheimer flow conditions
Re_c	Critical Reynolds number
d	Mean pore diameter, m
d_{eqv}	Equivalent pore diameter, m
k	Permeability, mD
q	Gas flow rate, m ³ /d
q_D	Volumetric flow rate related to Darcy flow conditions, m ³ /d
q_{Dm}	Mass flow rate related to Darcy flow conditions, kg/d
q_F	Volumetric flow rate related to Forchheimer flow conditions, m ³ /d
q_{Fm}	Mass flow rate related to Forchheimer flow conditions, kg/d
r_e	External drainage radius, m
r_w	Wellbore radius, m
u	Velocity, m/s
u_D	Volumetric velocity related to Darcy flow conditions, m/s
u_{Dm}	Mass velocity related to Darcy flow conditions, kg/(s m ²)
u_F	Volumetric velocity related to Forchheimer flow conditions, m/s
u_{Fm}	Mass velocity related to Forchheimer flow conditions, kg/(s m ²)
h	Formation thickness, m
$\text{grad } P$	Pressure gradient, Pa/m
r	Pore throat radius in Table 2, m
x	Linear coordinate, m
R^2	Determination coefficient
B_1	Constant in Eq. 20
a	Constants in Table 1
b	Constants in Table 1
c	Constant in Eq. 4
c'	Constant in Eq. 5
a, b, c	Coefficients in Eq. 34
a_1, b_1, c_1	Coefficients in Eq. 57

Greek Letters

α	Constant in Eq. 20
β	Non-Darcy coefficient, m ⁻¹
γ	Weak inertia factor
λ	New turbulent flow correlation factor, ft
μ	Viscosity, Pa s
ρ	Density, kg/m ³
ρ_0	Density at standard conditions, kg/m ³

τ	Tortuosity
ϕ	Porosity, fraction

Subscripts

D	Related to Darcy flow conditions
F	Related to Forchheimer flow conditions
c	Critical
e	External
eqv	Equivalent
exp	Experiment
m	Mass
p	Particles
sim	Simulation
t	Throat
w	Well

1 Introduction

For more than a century, Darcy's law serves as a fundamental rule of fluid flow through porous media. It became generally accepted that Darcy's law plays the same role as Ohm's law for electricity, Fourier's law for heat conduction, and Fick's law for diffusivity. Gas flow in porous media has received great attention due to its importance in the areas of pneumatic test analysis (Ahlers et al. 1995), soil depressurization systems (Fuente et al. 2019), transport and recovery of pollutants in water system (Ghane et al. 2014), and many other important areas of application. A basic law linking the pressure drop and velocity of fluid flow through porous media is Darcy's law (1856). It can be used for flows of gases, liquids, and mixtures. For a one-directional steady-state flow of an incompressible Newtonian fluid through a horizontal porous medium, it can be written as:

$$-\text{grad } P = \frac{\mu}{k} u. \quad (1)$$

However, several experimental results (Hubbert 1956; Wu et al. 1998; Zeng and Grigg 2006; Firouzi et al. 2014) show that this law can be used only in a narrow range of flow rates. Indeed, when the flow rate increases, the seepage velocity is no longer proportional to the pressure drop. On the contrary, as the pressure gradient decreases, the slip effect occurs, especially in low permeability media (Klinkenberg 1941).

Traditionally, two types of criteria, namely the Reynolds number and the Forchheimer number, have been used in the past to identify the beginning of a non-Darcy flow (Skjetne and Auriault 1999; Zeng and Grigg 2006; Macini et al. 2011; Ghane et al. 2014). Some authors believe that an advanced method is needed to understand and predict the non-Darcy flow and its characteristics, as it is critical for estimating the reduction in well productivity and reserve recovery (Huang and Ayoub 2008; Zolotukhin and Gayubov 2019). Concerns regarding deviations from Darcy's law in gas reservoirs have been expressed as early as the 1970s, but special attention was given to the wellbore zone (Holditch and Morse, 1976).

As the flow velocity increases, inertial forces become more significant (weak inertia), and the relationship between the pressure gradient and seepage velocity becomes

nonlinear. In this case, Darcy's law is generally corrected by a cubic term in seepage velocity (Firoozabadi and Katz, 1979).

$$-\text{grad } P = \frac{\mu}{k}u + \frac{\gamma}{\mu}\rho^2u^3. \quad (2)$$

Weak inertia is a rule in which the inertial force is of the same order as the viscous force. First, this deviation from Darcy's law was presented numerically by Firoozabadi and Katz (1979) and then theoretically derived for homogeneous isotropic media by Mei and Auriault (1991). Wodie and Levy (1991) analytically derived this law for homogeneous isotropic and space-periodic porous media by double-scale homogenization. The existence of a weak inertia rule is also numerically confirmed by Rasoloarijaona and Auriault (1994) and Skjetne (1995) and then experimentally by Skjetne and Auriault (1999).

At a high Reynolds number (strong inertial rule), the empirical Forchheimer equation (Forchheimer 1901) is used to account for the deviation from Darcy's law:

$$-\text{grad } P = \frac{\mu}{k}u + \beta\rho u^2. \quad (3)$$

Different names have been used for the β term in the literature. In this paper, we use the term "non-Darcy coefficient" when referring to β as it appears in the Forchheimer equation. This is an empirical value, the determination method of which is poorly studied, but it represents the inertial resistance in a porous medium and depends on the pore geometry and fluid properties.

A common problem in technology and science is the derivation of simple equations describing complex phenomena. Complex control equations are often known, but they are too difficult to analyze. The purpose of this study is to develop a simple flow model based on classical approaches and modern techniques such as dimensional analysis and machine learning methods. This method can be additionally used for fluid flow at low pressure gradients when the effect of gas slippage prevails over inertial forces. The focus of this article is on accounting for non-Darcy flow when inertial forces become more significant and the relationship between pressure gradient and seepage velocity becomes nonlinear.

The use of the above methods in a single combination allowed us to take a fresh look at complex processes in a porous medium. The study consists of two parts. In the first part, we briefly recall Darcy's and Forchheimer's laws and consider the issue of detecting the transition between the ranges of their applicability. The initial theoretical equations are estimated, and empirical dependencies are proposed based on the study of available data in the literature.

The second part is devoted to a more detailed consideration of the experimental data on determining the permeability of clastic consolidated porous samples. A correlation is presented for the non-Darcy flow coefficient concerning permeability, porosity, and tortuosity. Then, we briefly recap a derivation of a semi-analytical equation using the regression machine learning method. A comparison of the experimental results with the proposed model showed good agreement between them over the whole range of basic reservoir and fluid parameters. Studies have also shown that there is a transition zone from linear to a nonlinear flow rule, which is determined by the interval of Forchheimer numbers. The use of the Forchheimer number made it possible to identify a universal law of fluid flow through a porous medium in a simple analytical form valid for any flow geometry. The results of macro-modeling show that in the case of a gas reservoir, the gas flow in the entire

reservoir area deviates from Darcy's law. This effect can be significant when assessing the effectiveness of the gas reservoir performance.

2 Data and Analysis Methods for Nonlinear Fluid Flow Behavior

Experimental studies have shown that the β coefficient is related in various ways to rock properties, such as porosity, permeability, tortuosity, specific surface area, grain and pore size distribution, and surface roughness, rather than fluid properties.

In some cases, permeability alone does not correlate very well with the non-Darcy coefficient. Noman et al. (1985) conducted an experimental study on two core plugs with the same permeabilities and found that they have a significant difference in β values. They concluded that other rock properties should be included in the β correlation. In determining the non-Darcy coefficient from the correlation of permeability and type of porosity, the identified permeability still had an inverse relationship with β . Porosity exhibits a more complex relationship: In some experiments, it appears to be inversely proportional to β , while in others, it is directly proportional. The following section reviews the literature related to the Forchheimer model and the available correlations of the non-Darcy coefficient.

The first experimental data on non-Darcy flow appeared in the literature in the early 1930s. Table 1 lists the most interesting empirical relationships. Note that the cases considering a non-Darcy flow in a multiphase system (Wong 1970; Kutasov 1993; Frederick and Grave 1994; Coles and Hartman 1998) were not included in our study. Many of those equations were obtained for different rock types. From theoretical Eqs. 4 and 5, derived for different pore geometries by Irmay (1958) and Geertsma (1974), respectively, we see that they are very different from each other.

$$\beta = \frac{c}{k^{0.5}\phi^{1.5}} \quad (4)$$

$$\beta = \frac{c'\tau}{k\phi}. \quad (5)$$

It should be noted that Eqs. 1–3 are applicable for certain rules of fluid flow in a porous medium. Figure 1 shows a graph of various flow rules from the effect of gas slippage (first part of area 1) to the display of the turbulence effect in a porous medium (Skjetne 1995).

It would be desirable to have criteria that separate and quantify the full range of fluid flows in a porous medium shown in Fig. 1. The rule criterion is required to determine the beginning of the non-Darcy flow. Two types of criteria, the Reynolds number (Re) and the Forchheimer number (Fo), have been introduced earlier for identifying the beginning of the non-Darcy flow (Ruth and Ma 1992; Skjetne and Auriault 1999; Zeng and Grigg 2006; Ghane et al. 2014).

The Reynolds number Re is defined as the ratio of inertial to viscous forces:

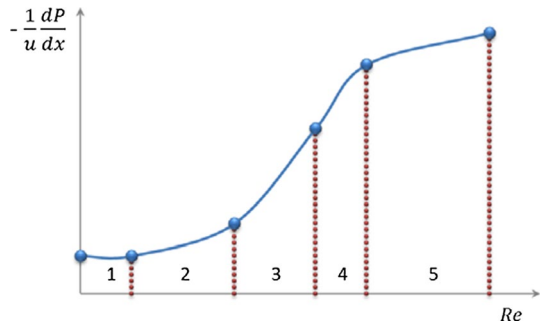
$$\text{Re} = \frac{\rho u d}{\mu}. \quad (6)$$

Table 2 summarizes the correlations used to estimate the Reynolds number obtained by different researchers.

Table 1 Literature summary of equations estimating the non-Darcy coefficient

No.	Empirical model β	Units of k and β	Source
1	$\beta = ab^{-\frac{1}{2}}(10^{-8}k)^{-\frac{1}{2}}\phi^{-\frac{3}{2}}$ where $a = 1.75; b = 150$	D, cm^{-1}	Ergun (1952)
2	$\beta = 1.82 \cdot 10^8 k^{-\frac{5}{4}} \phi^{-\frac{3}{4}}$	mD, cm^{-1}	Janicek and Katz (1955)
3	$\beta = 5.5 \cdot 10^9 k^{-\frac{5}{4}} \phi^{-\frac{3}{4}}$	mD, ft^{-1}	Tek et al. (1962)
4	$\beta = 0.005k^{-0.5}\phi^{-5.5}$	$\text{cm}^2, \text{cm}^{-1}$	Geertsma (1974)
5	$\beta = ab^{-\frac{1}{2}}(10^{-8}k)^{-\frac{1}{2}}\phi^{-\frac{3}{2}}$ $a = [1.8 \sim 4]; b = 180$	D, cm^{-1}	MacDonald et al. (1979)
6	$\beta = 1.47 \cdot 10^7 k^{-0.55}$ (unconsolidated) $\beta = 2.33 \cdot 10^{10} k^{-1.201}$ (consolidated)	mD, ft^{-1}	Brown (1980)
7	$\beta = 6.15 \cdot 10^{10} k^{-1.55}$ $\beta = 3.13 \cdot 10^{12} k^{-1.78} \phi^{-1.78}$	mD, ft^{-1}	Jones (1987)
8	$\beta = 8.91 \cdot 10^8 k^{-1} \phi^{-1} \tau$	mD, ft^{-1}	Liu et al. (1995)
9	$\beta = 1.55 \cdot 10^4 \tau^{3.35} k^{-0.98} \phi^{-0.29}$ $\beta = 2.5 \cdot 10^5 k^{-1}$ $\beta = 3.1 \cdot 10^4 \tau^3 k^{-1}$	D, cm^{-1}	Thauvin and Mohanty (1998)
10	$\beta = 1.07 \cdot 10^{12} k^{-1.88} \phi^{0.449}$ (same porosity method) $\beta = 2.49 \cdot 10^{11} k^{-1.79} \phi^{0.537}$ (simultaneous equations)	mD, ft^{-1}	Coles and Hartman (1998)
11	$\beta = 10^{-3.25} k^{-1.023} \tau^{1.943}$	$\text{cm}^2, \text{cm}^{-1}$	Cooper et al. (1999)
12	$\beta = 11,500k^{-1}\phi^{-1}$	D, cm^{-1}	Li and Engler (2001)
13	$\beta = \lambda Fk^{-1}$	D, ft^{-1}	Kollbotn and Bratteli (2005)
14	$\beta = 4.1 \cdot 10^{11} k^{-1.5}$	mD, m^{-1}	Friedel and Voigt (2006)
15	$\beta = 10^{-3} \tau^{1.1} k^{-1} \phi^{3.2} d$	$\text{m}^2, \text{m}^{-1}$	Choi and Song (2019)

Fig. 1 Flow rules in porous media. 1—Darcy’s law; 2—weak inertia; 3—Forchheimer (strong inertia); 4—transition from Forchheimer to turbulence; 5—turbulence (Skjetne 1995)



Cornell and Katz (1953) related the non-Darcy effect to turbulence or nonlinearity between the pressure gradient and the flow velocity. However, many studies, such as Bear (1972), Scheidegger (1974), Barak (1987), Ruth and Ma (1992), and Whitaker (1996), have concluded that nonlinearity is associated not with turbulence but rather with inertial effects. Kadi (1980) often used the terms “non-Darcy” and “turbulent” in gas flow technology to describe visco-inertial flow at high velocities near the wellbore region of gas wells. Bear (1972) systematically cited three reasons to exclude turbulence as the cause for the non-Darcy effect:

Table 2 Literature summary of the Reynolds number equations

Formula		Critical Reynolds number	Authors
$Re = \frac{u \cdot d_{\text{eqv}} \cdot \rho}{(0.75\phi + 0.23)\mu}$	(7)	$7.5 \leq Re_c \leq 9.0$	Pavlovskiy (1922)
$Re = \frac{\rho D_p u}{\mu}$	(8)	$40 \leq Re_c \leq 80$	Chilton and Colburn (1931)
$Re = \frac{\rho D_p u}{\mu}$	(9)	$10 \leq Re_c \leq 1000$ (unconsolidated) $0.4 \leq Re_c \leq 3$ (loosely consolidated)	Fancher and Lewis (1933)
$Re = \frac{u \rho \sqrt{k}}{\phi^{1.5} \mu}$	(10)	$0.02 \leq Re_c \leq 0.29$	Millionshikov (1935)
$Re = \frac{10u \rho \sqrt{k}}{\phi^{2.5} \mu}$	(11)	$1 \leq Re_c \leq 12$	Shelkachev and Lapuk (2001)
$Re = \frac{k \beta \rho u}{\mu}$	(12)	$0.1 \leq Re_c \leq 0.2$	Green and Duwez (1951)
$Re = \frac{\rho D_p u}{\mu} \frac{1}{1-\phi}$	(13)	$3 \leq Re_c \leq 10$	Ergun (1952)
$Re = \frac{\rho D_p u}{\mu}$	(14)	$3 \leq Re_c \leq 10$	Ma and Ruth (1993)
$Re = \frac{\rho u}{\mu}$	(15)	$Re_c = 0.11$	Thauvin and Mohanty (1998)

1. In turbulent flow-through pipes, the linear term in Eq. 2 does not exist;
2. In the flow-through pipes, the transition from laminar to turbulent flow is not gradual but rather abrupt;
3. The critical Reynolds number Re_c , at which the transition begins, is several orders of magnitude higher than the value at which the non-Darcy effect begins.

For the third reason mentioned above, Ruth and Ma (1992) provided an example illustrating the idea that the non-Darcy flow does not necessarily imply a high microscopic Reynolds number. They argued that in a straight tube model, non-Darcy effects do not become apparent until true turbulence sets in at $Re \approx 2000$, while in the curved tube model, microscopic inertial effects occur early at $Re \approx 1$. They concluded that the non-Darcy effect occurs because microscopic inertial effects change the velocity and pressure fields. Further on, it became evident that non-Darcy flow occurs not only in gas reservoirs, fractured reservoirs, and multipermeability systems but also in oil reservoirs that experience nonlinearity due to non-Darcy flow behavior (Belhaj et al. 2003).

In addition to the Reynolds number, it was proposed to use a Forchheimer number as a criterion for the transition from linear to nonlinear fluid flow in porous media (Ruth and Ma 1992). The Forchheimer number Fo is defined as the ratio of the pressure gradient required to overcome inertial forces to that of viscous forces:

$$Fo = \frac{k \beta \rho u}{\mu}. \quad (16)$$

Zeng and Grigg (2006) suggested a relationship between the non-Darcy effect E and the Forchheimer number Fo :

$$E = \frac{Fo}{1 + Fo}. \quad (17)$$

They demonstrated that the Forchheimer number is a better criterion than the Reynolds number for non-Darcy flows in porous media. In their study, the critical condition for the onset of flow nonlinearity was defined as the point where the non-Darcy effect E_c reaches 10%, which corresponds to a critical Forchheimer number Fo_c equal to 0.11. Macini et al.

(2011) used Fo_c in the range from 0.22 to 0.56, which corresponds to the value of E_c from 13 to 38%. Ghane et al. (2014) also estimated the Fo_c in the range of 0.14 to 0.55 (E_c from 12 to 36%). Our analysis shows that the range of critical values of Fo , which defines a transition zone from linear to non-Darcy flow, is more appropriate in this case. According to our estimates (see details in Sect. 3), the critical Forchheimer number ranges from 0.08 to 0.27, and the non-Darcy effect E ranges from 7 to 21% for all core samples.

3 Experimental Data and Methods

In our previous study (Zolotukhin and Gayubov 2019), various machine learning methods were used to obtain a modified Forchheimer equation for a wide range of porous medium parameters and pressure gradients. The authors analyzed the data of clastic reservoir samples with permeabilities ranging from 12 to 1132 mD available in the literature (Tessem 1980; Torsæter et al. 1981). It should be noted that the experiments of Tessem and Torsæter et al. were conducted for a single-phase flow.

Two methods of machine learning were considered, namely artificial neural networks (ANNs) and multiple regression models (MLRs). When processing the experimental data, it was necessary to preset the approximate value of the permeability to determine the non-Darcy coefficient. For this purpose, ANNs were used; porous media properties such as porosity, sample length, pressure drop, and fluid flow rate were represented as input layers in the ANN model, while permeability was the output layer in the training model. As a result, it was possible to train a neural network with four hidden layers containing 11 neurons each. The determination coefficient (R^2) between the estimated permeability and the actual core permeability was 0.92. Based on these results, the ANN model was selected to predict permeability. Many previous studies have focused on permeability and porosity prediction using artificial intelligence (AI), which were discussed in detail by Ansah et al. (2020). These results showed the effectiveness of this method in solving such problems.

The second method, MLR, in combination with dimensional analysis, found its application in obtaining the universal equation of fluid flow in a porous medium. This, in turn, enables high accuracy and reliability of predicted flow rules over the entire range of pressure gradients under both experimental and reservoir conditions. Besides, this method is the simplest in machine learning and effective in finding dependencies between input and predicted parameters. By applying the MLR method, we secured a high value of the determination coefficient $R^2 = 0.98$.

Using the methods above, discussed in detail in Zolotukhin and Gayubov (2019) and new data, it is possible to obtain the following modified Forchheimer equation (semi-analytical equation):

$$-\text{grad } P = \frac{\mu}{k} u + \tau \cdot \frac{1}{\sqrt{k} \phi^{1.5}} \rho u^2 \quad (18)$$

where τ is the tortuosity, which is determined as follows:

$$\tau = B_1 \cdot \left(\frac{\phi l^2}{k} \right)^\alpha \quad (19)$$

Here, B_1 and α are constants equal to $9.67 \cdot 10^{-5}$ and 0.47, respectively. To obtain a semi-analytical expression for a flow rate, comparing Eqs. 3 and 18, we obtain the following

expression for the non-Darcy coefficient, which is advantageous in that both hydraulic properties of the rock and the fluid properties are considered simultaneously:

$$\beta = B_1 \cdot \left(\frac{\phi l^2}{k}\right)^\alpha \cdot \frac{1}{\sqrt{k}\phi^{1.5}} = \tau k^{-0.5} \phi^{-1.5}. \tag{20}$$

Many authors include the tortuosity parameter in the Forchheimer equation (Bear 1972; Thauvin and Mohanty 1998; Cooper et al. 1999; Muljadi et al. 2016; Choi and Song 2019, Gjengedal et al. 2020). Note that Darcy’s law does not include the concept of pore tortuosity. This can be explained by the fact that the range of pressure drops and velocities in Darcy’s experiments was such that the inertial forces associated with tortuosity did not occur. Similar reasons were also given by Hubbert (1956). With the assistance of MLR, it has been proven that the inclusion of tortuosity helps to improve the correlation of experimental data to Eq. 18. The estimates made using Eq. 20 show that tortuosity for a wide range of reservoir parameters is bounded by the following values: $1.15 \leq \tau \leq 8.83$. This result is close to the estimates made in Cooper et al. (1999) and Muljadi et al. (2016). It should be recalled that tortuosity is a parameter that characterizes a porous medium at a mesoscale and is determined based on laboratory studies conducted on cores.

The use of dimensional analysis (Zolotukhin and Ursin 2000a, b) and machine learning methods (Zolotukhin and Gayubov 2019) leads to the following equation for the Reynolds number:

$$Re = \frac{u\rho\sqrt{k}}{\mu\phi^{1.5}}. \tag{21}$$

The analysis shows that the critical Reynolds number identifying transition to non-Darcy flow is in the range of 0.01–0.2. Note that Eq. 21 is similar to Eq. 10 obtained earlier by Millionshikov (1935).

Although the Reynolds number plays an important role in the formation of various modes of fluid flow, it should be noted that the Forchheimer number is more general, since it includes both the Reynolds number and tortuosity. Several researchers have expressed their preference for using this type of criterion (Geertsma 1974; Martins et al. 1990; Gidley 1991). Therefore, we consider the Forchheimer number as a flow rule criterion in our studies. Using Eqs. 16, 19, and 21, we obtain a new definition of the Forchheimer number in terms of tortuosity and Reynolds number:

$$Fo = \beta \cdot \frac{k\rho u}{\mu} = \frac{\tau}{\sqrt{k}\phi^{1.5}} \cdot \frac{k\rho u}{\mu} = \tau \cdot \frac{u\rho\sqrt{k}}{\mu\phi^{1.5}} = \tau \cdot Re. \tag{22}$$

Table 3 contains information on basic physical characteristics of porous media, and their derivatives (non-Darcy coefficient, critical Reynolds number, critical Forchheimer number, and critical non-Darcy effect) based on the total of 203 experimental data points collected and described in a previous study (Zolotukhin and Gayubov 2019). Figure 2 shows the plots of the non-Darcy coefficient as a function of porosity, permeability, tortuosity, and Forchheimer number. The graphs indicate that β is inversely proportional to the porosity (weak correlation) and permeability (strong correlation). Furthermore, the non-Darcy coefficient increases with increasing tortuosity and decreases with the Forchheimer number (strong correlations).

Table 3 Basic physical characteristics of the samples of the porous medium and their derivatives

No.	k , mD	ϕ	l , m	τ	β , m^{-1}	Re_c	Fo_c	E_c
1	1132.00	0.204	0.051	1.152	1.18E+07	0.135	0.156	0.135
2	254.00	0.188	0.051	2.238	5.45E+07	0.076	0.170	0.145
3	177.68	0.192	0.051	2.674	7.54E+07	0.068	0.182	0.154
4	174.91	0.202	0.051	2.759	7.27E+07	0.076	0.210	0.173
5	173.89	0.192	0.052	2.721	7.76E+07	0.079	0.215	0.177
6	165.28	0.173	0.051	2.620	8.96E+07	0.087	0.228	0.186
7	135.88	0.147	0.051	2.675	1.29E+08	0.099	0.265	0.209
8	101.40	0.184	0.051	3.405	1.35E+08	0.064	0.218	0.179
9	85.83	0.201	0.049	3.719	1.41E+08	0.057	0.212	0.175
10	22.65	0.202	0.051	7.197	5.27E+08	0.015	0.108	0.097
11	16.03	0.149	0.051	7.352	1.01E+09	0.011	0.081	0.075
12	13.97	0.169	0.051	8.322	1.01E+09	0.013	0.108	0.098
13	12.14	0.162	0.052	8.826	1.23E+09	0.009	0.079	0.074

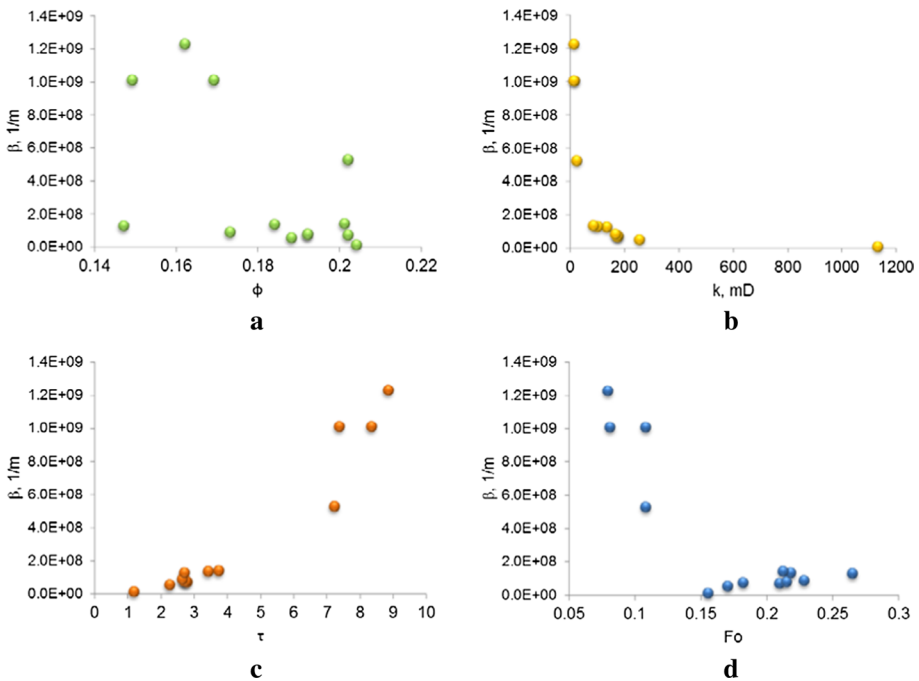


Fig. 2 Correlation of the non-Darcy coefficient with hydraulic properties such as porosity (a), permeability (b), tortuosity (c), and Forchheimer number (d)

The following sections of the article will focus on the different scales of observation of fluid flow and the effects associated with non-Darcy flows.

3.1 Fluid Flow at Different Scales

The flow of fluids that occurs in the partial volume of porous rock, even if very small, can only be described qualitatively because of the great complexity of the phenomenon. However, there are some regularities in the behavior of a rock–fluid system that can be described in terms of continuum mechanics. Let us consider the flow of fluids in a natural reservoir, with the scale of the flow ranging from very small to large (Fig. 3). Under natural conditions, many physical phenomena (for example, effects of wettability, fluid viscosity, fluid adhesion, clay swelling, tortuosity, impurity adsorption, polymer retention, etc.) occur at a scale of 10^{-4} – 10^{-2} m comparable to the rock’s grain or pore size (microscale) (Fig. 3a). At a larger scale, with elementary volumes considered on the order of 10^{-1} – 10^0 m, the effects of microscale phenomena listed above can be statistically “averaged” and readily quantified as constants or empirical relationships in equations of continuum mechanics (mesoscale) (Fig. 3b) (Zolotukhin and Ursin 2000a, b). The difference between the meso- and macro-modeling levels is not a change in the type of flow equations but rather a change in the scale of the models and averaging of geological and physical properties at new scales. A similar type of classification of models at various scales, namely at the micro-, meso-, and macro-levels, has been discussed in the literature from various points of view, such as structural geology (Morad et al. 2010) and field development (Homuth et al. 2015).

Well performance and productivity evaluation are fundamental to petroleum reservoir engineering at different phases of production. This task requires that physical and mathematical models adequately characterize the fluid flow in various geological settings. In this section, we use a semi-analytical model (modified Forchheimer equation) and conventional Darcy’s law to estimate the effect of nonlinearity on fluid velocities and flow rates in porous media at meso- and macroscales. First, we conduct this study at the mesoscale—a scale at which most of the experiments take place and where principles of continuum mechanics are widely used in hydrodynamic modeling. Then, the well production rates are estimated at the macroscale level (10^2 – 10^4 m).

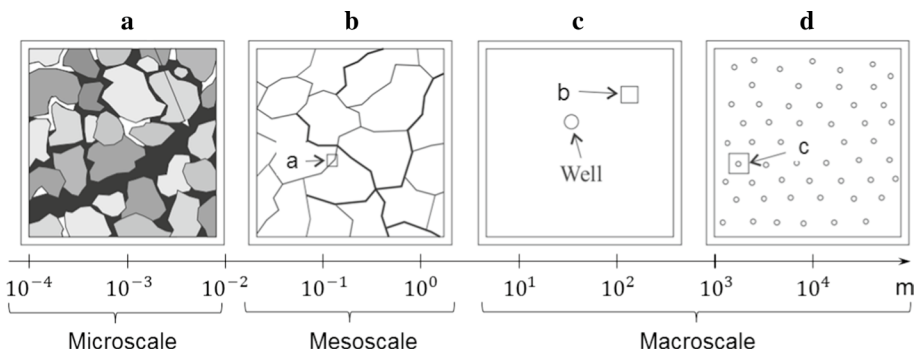


Fig. 3 Models of fluid flow in a porous medium at different scales of observation. **a** Microscale: grain and pore size; **b** mesoscale: rock sample size; **c** macroscale: interwell distance; **d** macroscale: reservoir or field size (Zolotukhin and Ursin 2000a, b)

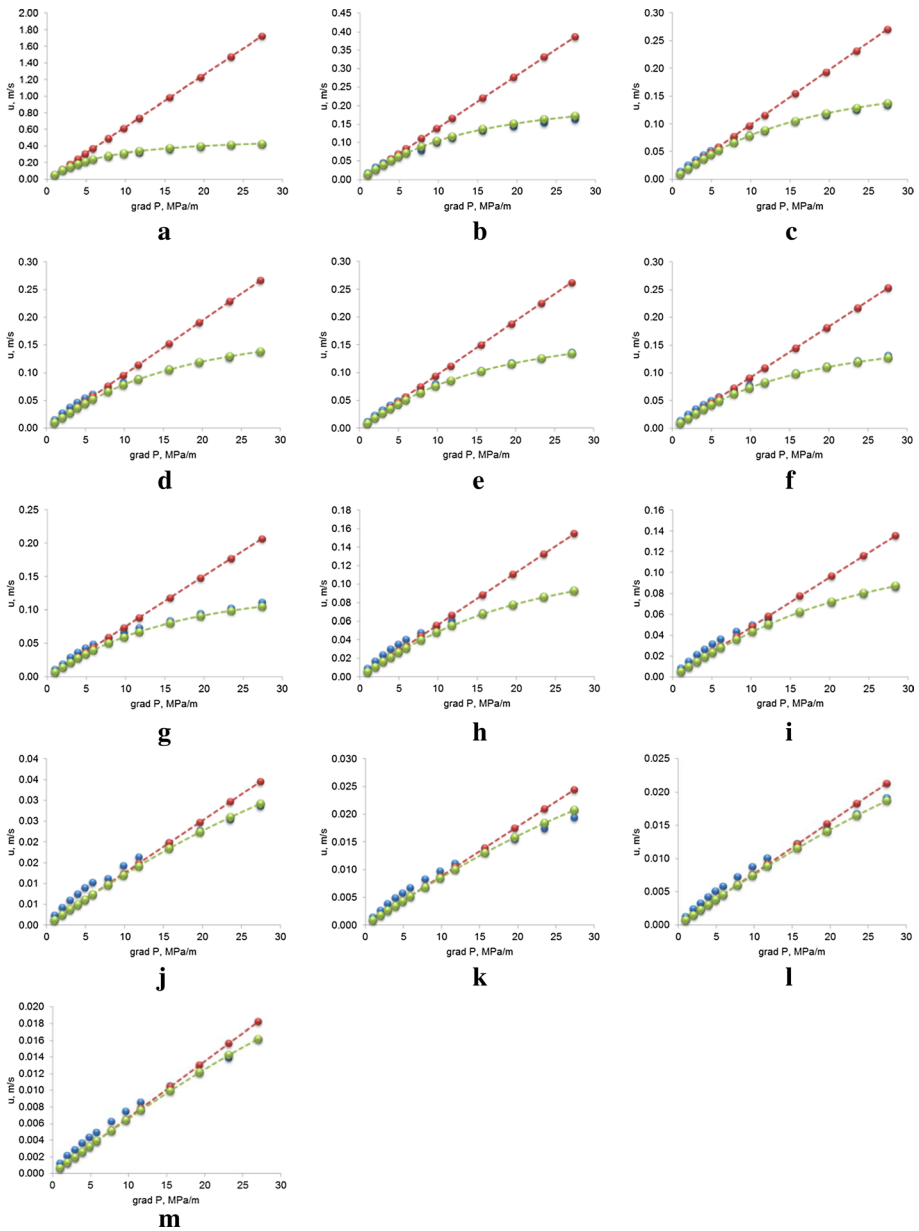


Fig. 4 Comparison of flow velocities calculated according to Darcy (red line) and modified Forchheimer equations (green line) with the experimental data (blue dots) of 13 tests (Tessem 1980; Torsæter et al. 1981) with permeabilities: **a** 1132 mD; **b** 254 mD; **c** 177.68 mD; **d** 174.91 mD; **e** 173.89 mD; **f** 165.28 mD; **g** 135.88 mD; **h** 101.4 mD; **i** 85.83 mD; **j** 22.65 mD; **k** 16.03 mD; **l** 13.97 mD; **m** 12.14 mD

3.2 Mesoscopic Model

Figure 4 shows the results of the calculation of flow velocities based on Darcy’s and modified Forchheimer’s flow rules (Eqs. 23–24) and their comparison with the experimental results of 13 tests (Tessem 1980; Torsæter et al. 1981). In tests on core samples with permeabilities of 12–1132 mD, excellent agreement between experimental results and numerical predictions is very obvious, specifically in the non-Darcy domain. Figure 4 shows that Darcy’s law is accurate in a rather narrow range of flow velocities. At a higher pressure gradient, the difference between the actual and calculated velocity values becomes significant, and Darcy’s law cannot be used. Note that the higher the reservoir permeability, the earlier the deviation from the linear law occurs.

By using Eqs. 1 and 3 written for the compressible linear steady-state flow at room temperature and assuming the perfect gas law $\rho(P) = \rho_0 \cdot P/P_0$, the following forms of the Darcy and modified Forchheimer equations can be written:

$$-\frac{k\rho_0}{\mu P_0} \cdot P \frac{dP}{dx} = \rho u_D \tag{23}$$

$$-\frac{k\rho_0}{\mu P_0} \cdot P \frac{dP}{dx} = \rho u_F + \tau \cdot \frac{\sqrt{k}}{\mu\phi^{1.5}} \rho^2 u_F^2. \tag{24}$$

Using the obvious definition $\rho u_F = u_{Fm} = \text{const}$, Eqs. 23 and 24 take the following forms:

$$-\frac{k\rho_0}{\mu P_0} \cdot P \frac{dP}{dx} = u_{Dm} \tag{25}$$

$$-\frac{k\rho_0}{\mu P_0} \cdot P \frac{dP}{dx} = u_{Fm} + \tau \cdot \frac{\sqrt{k}}{\mu\phi^{1.5}} u_{Fm}^2. \tag{26}$$

Integration of Eqs. 25 and 26 yields:

$$\int_{P_1}^P P \cdot dP = \frac{(P_1^2 - P^2)}{2} \tag{27}$$

and

$$\frac{k\rho_0}{\mu P_0} \cdot \frac{(P_1^2 - P^2)}{2} = u_{Dm} \cdot (x - x_1) \tag{28}$$

$$\frac{k\rho_0}{\mu P_0} \cdot \frac{(P_1^2 - P^2)}{2} = \left(u_{Fm} + \tau \cdot \frac{\sqrt{k}}{\mu\phi^{1.5}} u_{Fm}^2 \right) \cdot (x - x_1). \tag{29}$$

Equations 28 and 29 enable the calculation of pressure in a linear reservoir:

$$P_D(x) = \sqrt{P_1^2 - \frac{2\mu P_0}{k\rho_0} \cdot u_{Dm} \cdot (x - x_1)} \quad (30)$$

$$P_F(x) = \sqrt{P_1^2 - \frac{2\mu P_0}{k\rho_0} \cdot \left(u_{Fm} + \tau \cdot \frac{\sqrt{k}}{\mu\phi^{1.5}} u_{Fm}^2 \right) \cdot (x - x_1)}. \quad (31)$$

Here, subscripts F and D denote that the corresponding pressure distributions are calculated according to Darcy's and modified Forchheimer's laws. Note that the terms u_{Dm} and u_{Fm} should be evaluated with the Neumann boundary condition at $x = x_2$.

Usually, the following types of boundary conditions are used in solving differential equations:

- Conditions of the first kind, where the inlet and outlet pressure values are specified at the boundaries of the flow region (Dirichlet boundary conditions).
- Conditions of the second kind, where the pressure gradient or flow rate is set at the boundaries of the flow region (Neumann boundary conditions).
- Mixed conditions, when the condition of the first type is set on one of the boundaries (inlet) and the condition of the second type is set on the other (outlet).

In our simulation analysis, Dirichlet and mixed boundary conditions are used as the most appropriate for the considered tasks.

3.2.1 Boundary Condition of the First Kind (Dirichlet)

The following boundary condition is determined at the outflow boundary x_2 : $P(x_2) = P_2$. Then, Eqs. 28 and 29 can be solved for mass velocities that are still unspecified:

$$u_{Dm} = \frac{k\rho_0}{\mu P_0} \cdot \frac{(P_1^2 - P_2^2)}{2l} \quad (32)$$

$$u_{Fm} = \frac{-b + \sqrt{b^2 - 4ac}}{2a} \quad (33)$$

where

$$a = \tau \cdot \frac{\sqrt{k}}{\mu \cdot \phi^{1.5}}; b = 1; c = -\frac{k\rho_0}{\mu P_0} \cdot \frac{(P_1^2 - P_2^2)}{2l}. \quad (34)$$

The dimension of coefficients in Eq. 34 is as follows: $[a] = \text{m}^2 \text{ s kg}^{-1}$; $[c] = \text{kg m}^{-2} \text{ s}^{-1}$. Note that the last term in Eq. 34 is Darcy's mass velocity with a minus sign.

3.2.2 Mixed Boundary Condition

Let us change the boundary condition at the outlet section, i.e., $q_{Fm}(x_2) = q_{Dm}$. Since the mass flow rates are equal, we define the pressure distribution in the sample that

satisfies that condition. Then, Eqs. 35 and 36 can be solved for the pressure distribution for both flows:

$$P_D(x) = \sqrt{P_1^2 - \frac{2\mu P_0}{k\rho_0} \cdot u_{Dm} \cdot (x - x_1)} \tag{35}$$

$$P_F(x) = \sqrt{P_1^2 - \frac{2\mu P_0}{k\rho_0} \cdot \left(u_{Dm} + \tau \cdot \frac{\sqrt{k}}{\mu\phi^{1.5}} u_{Dm}^2 \right) \cdot (x - x_1)}. \tag{36}$$

For $x = x_2$, we obtain:

$$P_{D2} = \sqrt{P_1^2 - \frac{2\mu P_0}{k\rho_0} \cdot u_{Dm} \cdot l} \tag{37}$$

$$P_{F2} = \sqrt{P_1^2 - \frac{2\mu P_0}{k\rho_0} \cdot \left(u_{Dm} + \tau \cdot \frac{\sqrt{k}}{\mu\phi^{1.5}} u_{Dm}^2 \right) \cdot l}. \tag{38}$$

Figure 5 shows the results of a numerical simulation performed for the Dirichlet and Neumann outlet boundary conditions. In the first case (Fig. 5a), the outlet pressure P_2 is set equal to 0.1 MPa, and in the second case (Fig. 5b), the gas mass flow rate is set equal to 0.14 kg/(s m²) at the outlet. The results show that in the first case, the pressure distribution calculated using the Darcy and modified Forchheimer equations coincides, but the mass and volumetric flow rates are different ($u_{Fm}/u_{Dm} = 0.9$). In contrast, in the second case, the mass flow rates are identical, while the pressure distribution is different. This observation illustrates a well-known phenomenon called skin factor, which shows that in the case of nonlinear flow, an additional pressure drop is required to produce equally with Darcy flow.

Let us divide both parts of Eq. 33 by u_{Dm} :

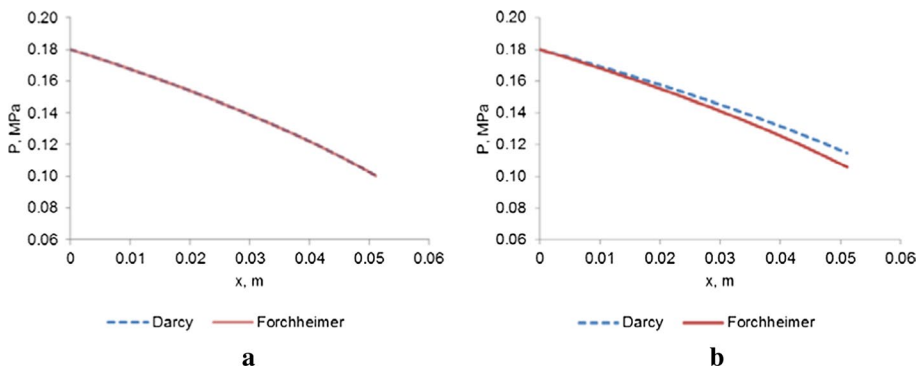


Fig. 5 Pressure distribution in the core sample with a permeability of 1132 mD. Dash blue line—Darcy equation; solid red line—modified Forchheimer equation. **a** Dirichlet outlet boundary condition ($P(x_2) = P_2$); **b** Neumann outlet boundary condition ($q_{Fm}(x_2) = q_{Dm}$)

$$\frac{u_{Fm}}{u_{Dm}} = \frac{-b + \sqrt{b^2 - 4ac}}{2a \cdot u_{Dm}}. \quad (39)$$

As seen from Eq. 34, $-a \cdot c = \tau \cdot \frac{\sqrt{k}}{\mu \cdot \phi^{1.5}} \cdot \frac{k\rho_0}{\mu\rho_0} \cdot \frac{(P_1^2 - P_2^2)}{2l} = \tau \cdot \frac{\sqrt{k}}{\mu \cdot \phi^{1.5}} \cdot u_{Dm} = \tau \cdot \text{Re}_D$. Further, using Eq. 22 in a form $\text{Fo}_D = \tau \cdot \text{Re}_D$ makes it possible to rewrite Eq. 39 in the following form:

$$\frac{u_{Fm}}{u_{Dm}} = \frac{\sqrt{(1 + 4\text{Fo}_D)} - 1}{2\text{Fo}_D}. \quad (40)$$

Since in laboratory experiments the ratio of mass and volumetric flows is the same at the core outlet ($u_{Fm} = u_{Dm}$), Eq. 40 can be rewritten in volumetric units:

$$\frac{u_F}{u_D} = \frac{\sqrt{(1 + 4\text{Fo}_D)} - 1}{2\text{Fo}_D}. \quad (41)$$

As follows from Eq. 41, the ratio ($u_F/u_D \leq 1$) indicates that Forchheimer velocity is always less than Darcy velocity and approaches it only when $\text{Fo}_D \rightarrow 0$.

Equation 41 can be simplified by replacing Fo_D with Fo . First, the terms Fo_D and Fo are defined as follows:

$$\text{Fo}_D = \tau \cdot \frac{\sqrt{k}}{\mu \cdot \phi^{1.5}} \cdot u_{Dm} = \tau \cdot \frac{\sqrt{k}}{\mu \cdot \phi^{1.5}} \cdot \rho \cdot u_D = \tau \cdot \text{Re}_D \quad (42)$$

$$\text{Fo} = \tau \cdot \frac{\sqrt{k}}{\mu \cdot \phi^{1.5}} \cdot u_{Fm} = \tau \cdot \frac{\sqrt{k}}{\mu \cdot \phi^{1.5}} \cdot \rho \cdot u_F = \tau \cdot \text{Re}_F. \quad (43)$$

Let us prove that the following equations are equivalent:

$$\frac{u_{Fm}}{u_{Dm}} = \frac{\sqrt{(1 + 4\text{Fo}_D)} - 1}{2\text{Fo}_D} \quad (44)$$

$$\frac{u_{Fm}}{u_{Dm}} = \frac{1}{1 + \text{Fo}}. \quad (45)$$

Since the left-hand terms in Eqs. 44 and 45 are identical, the following statement is valid:

$$\frac{1}{1 + \text{Fo}} = \frac{\sqrt{(1 + 4\text{Fo}_D)} - 1}{2\text{Fo}_D}. \quad (46)$$

Let us prove it. Equation 46 can be rewritten as:

$$\frac{2\text{Fo}_D}{1 + \text{Fo}} + 1 = \sqrt{(1 + 4\text{Fo}_D)}. \quad (47)$$

By squaring both sides of the equation, we obtain:

$$\left(\frac{2F_{oD}}{1+F_o}\right)^2 + \frac{4F_{oD}}{1+F_o} + 1 = 1 + 4F_{oD}. \tag{48}$$

Then, $\frac{F_{oD}}{(1+F_o)^2} + \frac{1}{1+F_o} = 1$ and

$$F_{oD} = F_o \cdot (1 + F_o). \tag{49}$$

Substituting the last result into the right-hand side of Eq. 44, we gradually obtain:

$\frac{\sqrt{(1+4F_{oD})}-1}{2F_{oD}} = \frac{\sqrt{1+4F_o(1+F_o)}-1}{2F_o(1+F_o)} = \frac{\sqrt{1+4F_o+4F_o^2}-1}{2F_o(1+F_o)} = \frac{\sqrt{(1+2F_o)^2}-1}{2F_o(1+F_o)} = \frac{1}{1+F_o}$, quod erat demonstrandum. Figure 6 shows the dependency of (u_{Fm}/u_{Dm}) on the pressure gradient and Forchheimer number Fo (Eq. 45).

After calculating the fluid flow rates, the following conclusions can be made:

- When solving the task for the Dirichlet boundary conditions, the pressure distribution in the sample remains the same. At the same time, mass and volumetric velocities can vary significantly depending on the given pressure drop.
- When solving the task with the outlet Neumann boundary condition, a fundamentally different result is obtained: For a given equal mass flow rate of gas, the calculated pressure distributions in the core following Darcy’s and modified Forchheimer’s laws differ significantly, and the Forchheimer outlet pressure is lower than that estimated by Darcy’s law.
- The fluid flow ratio (u_{Fm}/u_{Dm}) varies in the range from 99.9% (for permeability 12.14 mD) to 25% (for permeability 1132 mD).
- As the pressure gradient increases, the velocity ratio shown in Fig. 6a decreases significantly.
- It is important to note that for a wide range of permeability values, the experimental data perfectly fit the theoretical trend depicted in Fig. 6b and described by Eq. 45.

3.3 Macroscopic Model

In addition to the mesoscale model discussed above, a macroscopic model for radial flow has also been developed. Herein, we estimate the influence of the main reservoir (reservoir porosity, permeability, and tortuosity), fluid (oil and gas viscosity, and density), and technological parameters (pressure drawdown and well spacing) on the efficiency of field development.

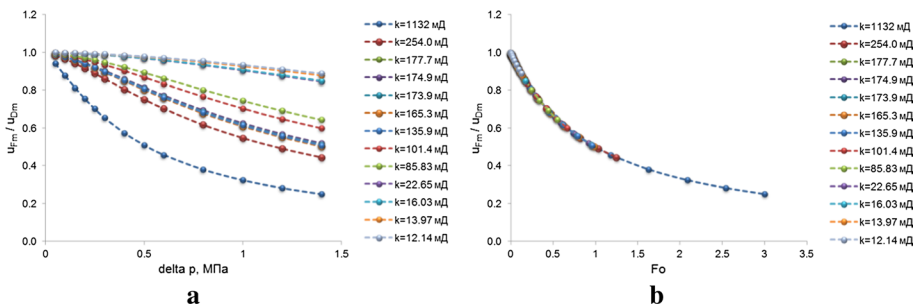


Fig. 6 Dependencies of the ratio (u_{Fm}/u_{Dm}) on the pressure gradient (a) and Forchheimer number Fo (b) based on the experimental results (Tessem 1980; Torsæter et al. 1981)

The well spacing is defined as the area of the field per production well and expressed in acres. Some of the reservoir properties (permeability, porosity, and tortuosity) are taken from Table 3. The rest of the reservoir and fluid characteristics, along with technological parameters, are summarized in Table 4.

The discussion in this part follows the logic of the previous section, where the linear flow of compressible gas is considered, i.e.,

$$\rho(P) = \frac{\rho_0}{P_0} P. \tag{50}$$

Let us write the equation of fluid flow (Eq. 18) for the radial geometry:

$$\frac{k}{\mu} \cdot \rho \frac{dP}{dr} = \rho u + \tau \cdot \frac{\sqrt{k}}{\mu \phi^{1.5}} \rho^2 u^2. \tag{51}$$

Using the obvious relation for the radial flow $u = \frac{q}{s} = \frac{q}{2\pi hr}$ and substituting it into Eq. 51, we obtain the following equation:

$$\frac{k}{\mu} \cdot \rho \frac{dP}{dr} = \frac{\rho q}{2\pi hr} + \tau \cdot \frac{\sqrt{k}}{\mu \phi^{1.5}} \left(\frac{\rho q}{2\pi hr} \right)^2. \tag{52}$$

Noting that $\rho q = q_m = \text{const.}$, Eq. 52 is as follows:

$$\frac{k}{\mu} \cdot \frac{\rho_0}{P_0} P \frac{dP}{dr} = \frac{q_m}{2\pi hr} + \tau \cdot \frac{\sqrt{k}}{\mu \phi^{1.5}} \left(\frac{q_m}{2\pi hr} \right)^2. \tag{53}$$

Separation of the variables and integration yields

$$\frac{k}{\mu} \cdot \frac{\rho_0}{P_0} \int_P^{P_c} P dP = \frac{q_m}{2\pi h} \cdot \int_r^{r_c} \frac{dr}{r} + \tau \cdot \frac{\sqrt{k}}{\mu \phi^{1.5}} \left(\frac{q_m}{2\pi h} \right)^2 \cdot \int_r^{r_c} \frac{dr}{r^2}$$

and further:

$$\frac{\pi kh}{\mu} \cdot \frac{\rho_0}{P_0} \cdot \frac{(P_c^2 - P^2(r))}{\ln \frac{r_c}{r}} = q_m + \tau \cdot \frac{\sqrt{k}}{\mu \phi^{1.5}} \cdot \frac{1}{2\pi h} \cdot \frac{1}{\ln \frac{r_c}{r}} \cdot \left(\frac{1}{r} - \frac{1}{r_c} \right) \cdot q_m^2. \tag{54}$$

Table 4 Reservoir, fluid, and technological parameters

No.	Parameter	Value				
1	Standard pressure ρ_0 , Pa	101,325				
2	Fluid density at standard conditions ρ_0 , kg/m ³	1.2				
3	Gas viscosity μ , Pa·s	3.1·10 ⁻⁵				
4	Reservoir pressure P_c , Pa	2.0·10 ⁷				
5	Flowing bottomhole pressure P_w , Pa	1.8·10 ⁷				
6	Formation thickness h , m	10				
7	Wellbore radius r_w , m	0.1				
8	External drainage radius r_c , m	169	239	339	479	677
9	Well spacing, acres	22.24	44.48	88.96	177.92	355.83

3.3.1 Boundary Condition of the First Kind (Dirichlet)

Solving the Dirichlet problem and setting the bottomhole pressure $P = P_w$ at $r = r_w$ enables us to find q_m :

$$\frac{\pi kh}{\mu} \cdot \frac{\rho_0}{P_0} \cdot \frac{(P_e^2 - P_w^2)}{\ln \frac{r_e}{r_w}} = q_{Fm} + \tau \cdot \frac{\sqrt{k}}{\mu \phi^{1.5}} \cdot \frac{1}{2\pi h} \cdot \frac{1}{\ln \frac{r_e}{r_w}} \cdot \left(\frac{1}{r_w} - \frac{1}{r_e} \right) \cdot q_{Fm}^2. \tag{55}$$

Using the following notation:

$$a_1 = \tau \cdot \frac{\sqrt{k}}{\mu \phi^{1.5}} \cdot \frac{1}{2\pi h} \cdot \frac{1}{\ln \frac{r_e}{r_w}} \cdot \left(\frac{1}{r_w} - \frac{1}{r_e} \right); b_1 = 1; c_1 = -\frac{\pi kh}{\mu} \cdot \frac{\rho_0}{P_0} \cdot \frac{(P_e^2 - P_w^2)}{\ln \frac{r_e}{r_w}} \tag{56}$$

Equation 55 can be rewritten in a compact form:

$$a_1 q_{Fm}^2 + b_1 q_{Fm} + c_1 = 0. \tag{57}$$

The solution to Eq. 57 can be written as:

$$q_{Fm} = \frac{-1 + \sqrt{1 - 4a_1 c_1}}{2a_1}. \tag{58}$$

Substituting the last result into Eq. 54 enables us to find the pressure distribution within the reservoir:

$$P_F(r) = \sqrt{\left(P_e^2 - \frac{\mu}{\pi kh} \cdot \frac{P_0}{\rho_0} \ln \frac{r_e}{r} \cdot q_{Fm} - \tau \cdot \frac{\sqrt{k}}{\mu \phi^{1.5}} \cdot \frac{1}{2\pi h} \cdot \frac{\mu}{\pi kh} \cdot \frac{P_0}{\rho_0} \cdot \left(\frac{1}{r} - \frac{1}{r_e} \right) \cdot q_{Fm}^2 \right)}. \tag{59}$$

Let us now define the mass flow rate of gas according to Darcy’s law:

$$q_{Dm} = \frac{\pi kh}{\mu} \cdot \frac{\rho_0}{P_0} \cdot \frac{(P_e^2 - P_w^2)}{\ln \frac{r_e}{r_w}}. \tag{60}$$

The corresponding pressure distribution is calculated as follows:

$$P_D(r) = \sqrt{\left(P_e^2 - \frac{\mu}{\pi kh} \cdot \frac{P_0}{\rho_0} \ln \frac{r_e}{r} \cdot q_{Dm} \right)}. \tag{61}$$

Figure 7 shows the results of calculations of pressures and flow rates for the linear and nonlinear laws of flow. The illustrations are presented in the form of pressures and flow relationships for different permeabilities and different well spacing values. Because the basic features of fluid flow are manifested in the near-wellbore zone, logarithmic grid coordinates are selected that allow the identification of those features and are calculated as follows:

$$\ln \frac{r_e}{r_w} = \ln \frac{r_e}{r_w} \cdot \frac{i}{n}, i = 0, 1, \dots, n, \tag{62}$$

where n is the number of intervals into which the reservoir is divided.

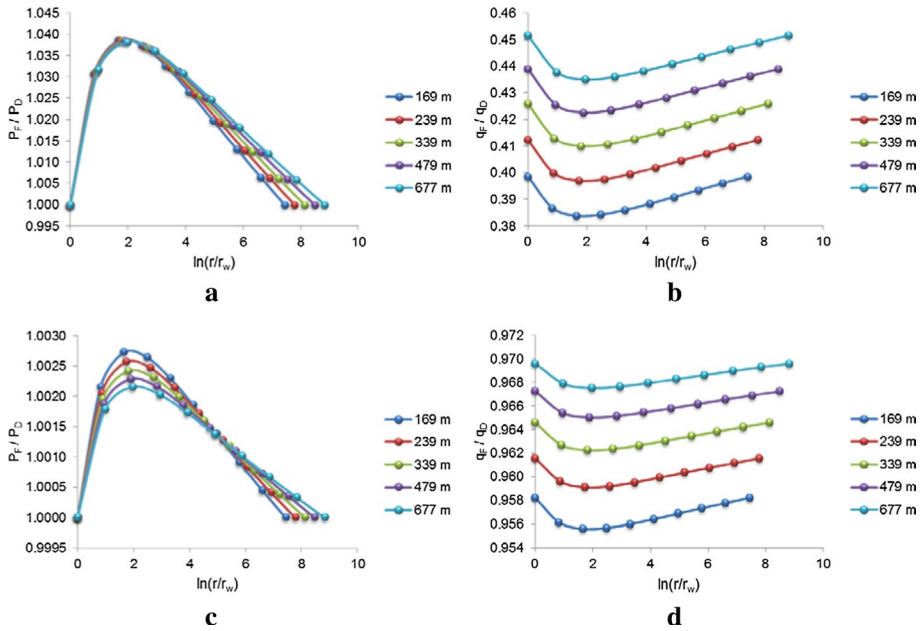


Fig. 7 Dirichlet boundary condition: the pressure P_F/P_D (**a**, **c**) and flow rates q_F/q_D (**b**, **d**) distribution ratio, calculated on the modified Forchheimer and Darcy rules for different well spacing values (169 m, 239 m, 339 m, 479 m, 677 m). Figures **a** and **b** correspond to reservoir permeability 1132 mD; **c** and **d** to 12.14 mD

As follows from the calculations, the higher the reservoir permeability, the higher the deviation of the distribution of pressure and flows from Darcy’s law. For example, the ratio of flow rates with a permeability of 12.14 mD varies from 0.956 to 0.970, while at a permeability of 1132 mD, this ratio decreases to 0.38–0.45 depending on the well spacing. The denser the well spacing, the greater the differences observed in the distribution of pressure and flow rates. Note that the highest changes in calculated parameters are observed in the interval from 25 cm to 15 m. This interval is much larger than the usual wellbore zone (10–50 cm).

3.3.2 Mixed Boundary Conditions

In this section, the gas flow rate is set as the Neumann wellbore boundary condition. Setting $q_{Fm} = q_{Dm}$ enables us to define the pressure distributions for modified Forchheimer’s and Darcy’s laws for different permeability values and well spacing parameters:

$$P_F(r) = \sqrt{\left(P_e^2 - \frac{\mu}{\pi kh} \cdot \frac{P_0}{\rho_0} \ln \frac{r_e}{r} \cdot q_{Fm} - \tau \cdot \frac{\sqrt{k}}{\mu \phi^{1.5}} \cdot \frac{1}{2\pi h} \cdot \frac{\mu}{\pi kh} \cdot \frac{P_0}{\rho_0} \cdot \left(\frac{1}{r} - \frac{1}{r_e} \right) \cdot q_{Fm}^2 \right)} \tag{63}$$

$$P_D(r) = \sqrt{\left(P_e^2 - \frac{\mu}{\pi kh} \cdot \frac{P_0}{\rho_0} \ln \frac{r_e}{r} \cdot q_{Dm} \right)}. \tag{64}$$

As follows from Fig. 8 (Neumann boundary condition), the highest changes in calculated parameters are observed in the interval from 25 cm to 15 m, which is larger than the usual wellbore zone (10–50 cm). It can be shown that relationships similar to Eqs. 42–46 can be obtained for the radial flow. Starting from the definitions of Fo_D and Fo , namely:

$$Fo_D = \tau \cdot \frac{\sqrt{k}}{\mu\phi^{1.5}} \cdot \frac{1}{2\pi h} \cdot \frac{1}{\ln \frac{r_e}{r_w}} \cdot \left(\frac{1}{r_w} - \frac{1}{r_e} \right) \cdot q_{Dm}, \tag{65}$$

$$Fo = \tau \cdot \frac{\sqrt{k}}{\mu\phi^{1.5}} \cdot \frac{1}{2\pi h} \cdot \frac{1}{\ln \frac{r_e}{r_w}} \cdot \left(\frac{1}{r_w} - \frac{1}{r_e} \right) \cdot q_{Fm}, \tag{66}$$

and following the logic of deriving Eq. 46, one obtains:

$$\frac{1}{1 + Fo} = \frac{\sqrt{(1 + 4Fo_D)} - 1}{2Fo_D} \tag{67}$$

Then, the ratio of the mass flow can be written as the following simple equation:

$$\frac{q_{Fm}}{q_{Dm}} = \frac{1}{1 + Fo}. \tag{68}$$

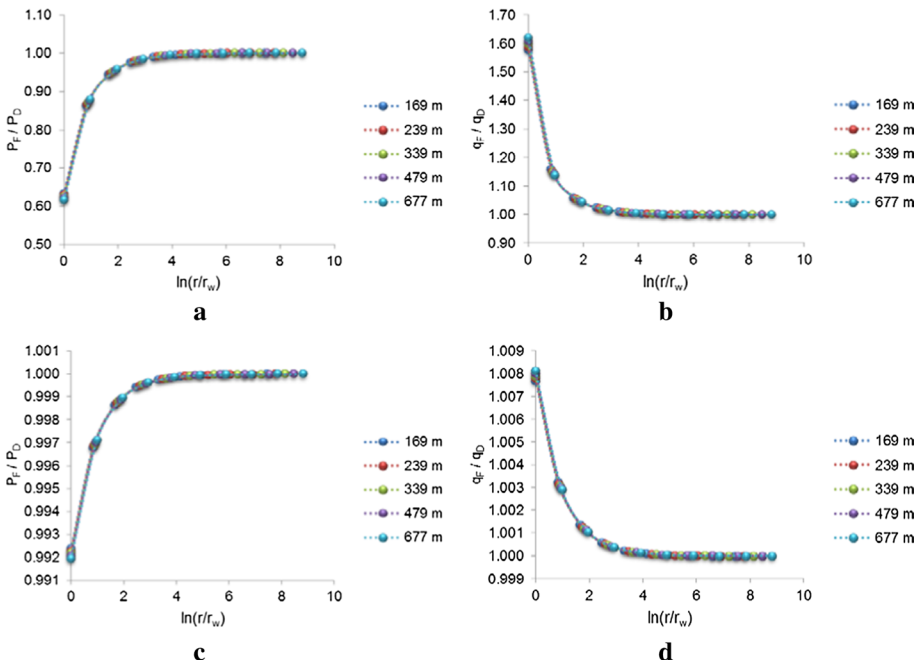


Fig. 8 Neumann wellbore boundary condition: the pressure P_F/P_D (a, c) and flow rates q_F/q_D (b, d) distribution ratio, calculated on modified Forchheimer and Darcy rules for different well spacing values (169 m, 239 m, 339 m, 479 m, 677 m). Figures a and b correspond to reservoir permeability 1132 mD; c and d to 12.14 mD

Figure 9 shows the results of calculating the dependence of the flow rate ratios (q_{Fm}/q_{Dm}) on the well spacing and the Forchheimer number (Fo).

The dependence of the mass flow rate ratio on the well spacing in Fig. 9a is similar to the linear flow geometry depicted in Fig. 6a. The fluid flow ratio (q_{Fm}/q_{Dm}) varies in the range from 99.9% (for permeability 12.14 mD) to 58% (for permeability 1132 mD). The dependency of (q_{Fm}/q_{Dm}) on the well spacing is much less pronounced compared to the permeability change. The effect of well spacing becomes more pronounced at high permeability values and practically disappears at low permeability. The results of calculations show that for a wide range of permeability values, the numerically generated data perfectly fit the theoretical trend depicted in Fig. 9b and described by Eq. 68. It should be noted that this equation includes the ratio of flow rates calculated using the modified Forchheimer and Darcy equations at the same pressure drops for any flow geometry.

4 Discussion

In this study, the following objectives were achieved: (1) developing a semi-analytical model describing non-Darcy behavior and (2) validating the model using the available data. The analysis conducted in the present work leads to the following conclusions:

- Numerous studies indicate that the numerical values of the β coefficient, determined experimentally, can vary up to ten thousand times, thereby indicating that the non-Darcy coefficient is not a coefficient but a parameter depending on the properties of a porous medium. The correlation between the hydraulic properties of the clastic core samples and the non-Darcy coefficient was analyzed using plots of key parameters used for predicting the β value (Fig. 2). The study indicates that β is inversely proportional to porosity (weak correlation), permeability, and Reynolds number (strong correlation), whereas it increases with increasing tortuosity. Finally, a correlation (Eq. 20) for the non-Darcy coefficient was derived.
- Note that tortuosity defined by Eq. 19 in a compact form is one of the important but not very well-defined parameters that affect the deviation from Darcy’s law. Further experiments are needed to assess the tortuosity of a porous medium, not only on linear cores but also on samples with different flow geometries and at different pressure.

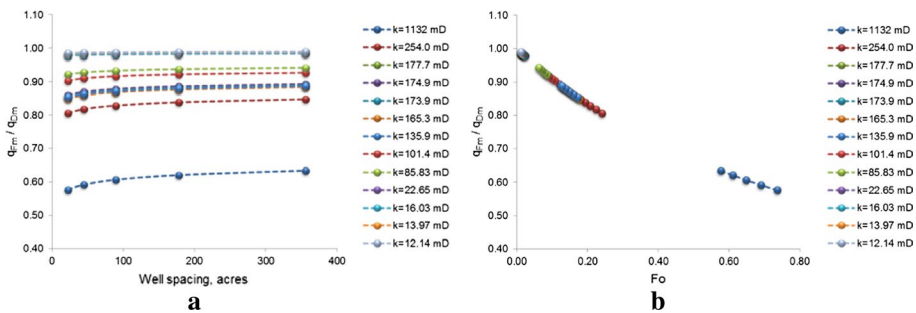


Fig. 9 Dependencies of the mass flow rate ratio (q_{Fm}/q_{Dm}) on well spacing (a) and Forchheimer number Fo (b) based on the experimental results of 13 tests (Tessem 1980; Torsæter et al. 1981) with permeability ranging from 1132 to 12.14 mD

Table 5 Reservoir characteristics and corresponding critical Forchheimer and non-Darcy coefficient numbers

No.	k , mD	τ	$Fo_{c\ exp}$	$E_{c\ exp}$	$Fo_{c\ sim}$	$E_{c\ sim}$
1	1132	1.152	0.156	0.135	0.100	0.091
2	254	2.238	0.170	0.145	0.092	0.084
3	177.68	2.674	0.182	0.154	0.083	0.077
4	174.91	2.759	0.210	0.173	0.107	0.097
5	173.89	2.721	0.215	0.177	0.112	0.101
6	165.28	2.620	0.228	0.186	0.100	0.091
7	135.88	2.675	0.265	0.209	0.100	0.091
8	101.4	3.405	0.218	0.179	0.108	0.097
9	85.83	3.719	0.212	0.175	0.120	0.107
10	22.65	7.197	0.108	0.097	0.105	0.095
11	16.03	7.352	0.081	0.075	0.101	0.092
12	13.97	8.322	0.108	0.098	0.107	0.097
13	12.14	8.826	0.079	0.074	0.098	0.089

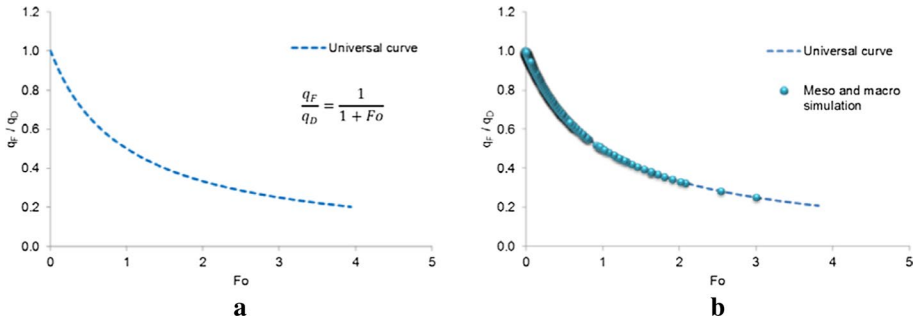


Fig. 10 Dependencies of the flow rate ratio (q_F/q_D) on Forchheimer number Fo . **a** Universal curve, **b** synthetic data (meso- and macro-modeling and universal curve)

- The critical Forchheimer numbers for each of the samples determined from the experimental data ($Fo_{c\ exp}$) and calculated using Eq. (22) ($Fo_{c\ sim}$) are presented in Table 5. These results confirm that there is no crisp number characterizing the transition from laminar to inertial flow, but there is a certain transition zone, the width of which depends on the reservoir and fluid properties.
- The results of macro-modeling show that in the case of a gas reservoir, the gas flow in the entire reservoir area differs from the Darcy’s law. As follows from the calculations, the higher the reservoir permeability, the higher the deviation of the distribution of pressure and flows rates from Darcy’s law. From the examples considered, it follows that a 10% deviation of the fluid flow ratio (q_F/q_D) is observed in reservoirs with permeability exceeding 100 mD, even at low pressure drops (20 atm) (Table 4). As follows from Fig. 9a, the deviation from the linear flow is observed for all values of the formation permeability (1132–12.14 mD), even at such a low pressure drawdown. Hence, non-Darcy flow effects in gas reservoirs should not be disregarded to avoid an overestimation of the forecasted gas production rates.

- Simulation results of compressible fluid flow on a macroscale show an interesting effect: The difference between the pressure distributions, calculated using modified Forchheimer's and Darcy's laws, reaches a maximum in the interval from 25 cm to 15 m, which is larger than the usual wellbore zone (10–50 cm).
- It was possible to obtain a universal equation (Eq. 68) for the ratio of flow rates at meso- and macroscales as a single function of the Forchheimer number. Figure 10 shows the results of all the calculations performed in this study, i.e., data on laboratory studies on core samples and numerical study for radial flow at different pressure drawdowns and well spacing. As follows from Fig. 10, the data obtained from the simulation exercise perfectly match the universal curve.

5 Conclusion

1. In this study, the application field and modified Forchheimer equation were presented, and the range of values and the physical significance of its parameters were analyzed.
2. Published relations for the β coefficient were considered (Table 1). The use of the approach based on dimensional analysis allowed expression of the β coefficient with a simple combination of tortuosity, permeability, and porosity (Eq. 20).
3. It was proven that non-Darcy effects should be considered to avoid an overestimation of the forecasted gas production rates.
4. Analysis of experimental data shows that the Forchheimer number plays a key role in describing flow in porous media. The use of the Forchheimer number made it possible to identify the universal law of fluid flow through a porous medium in a simple analytical form valid for any flow geometry (Eq. 68).

6 Availability of Data and Material

All data generated or analyzed during this study are included in this published article.

Author's Contributions All authors contributed to the study conception and design. Material preparation, data collection, and analysis were performed by ABZ and ATG. The first draft of the manuscript was written by ABZ and ATG, and all authors commented on previous versions of the manuscript. All authors read and approved the final manuscript. ABZ conceived the study and contributed to project administration, supervision, and validation. ABZ and ATG curated the data, performed the formal analysis, and contributed to investigation, methodology, resources, and writing—review and editing. Funding acquisition is not applicable. ATG contributed to software, visualization, and writing—original draft.

Funding Not applicable.

Code Availability Code sharing is not applicable to this article as no software application or custom code was generated or analyzed during the current study.

Compliance with Ethical Standards

Conflict of interest The authors declare that they have no conflict of interest.

References

- Ahlers, C.F., Finsterle, S., Wu, Y.S., Bodvarsson, G.S.: Determination of pneumatic permeability of a multi-layered system by inversion of pneumatic pressure data. In: Proceedings of the 1995 AGU Fall Meeting. San Francisco, California (1995)
- Ansah, E.O., Vo Thanh, H., Sugai, Y., Ngele, R., Sasaki, K.: Microbe-induced fluid viscosity variation: field-scale simulation, sensitivity and geological uncertainty. *J. Petrol. Explor. Prod. Technol.* **10**, 1983–2003 (2020). <https://doi.org/10.1007/s13202-020-00852-1>
- Barak, A.Z.: Comments on 'high velocity flow in porous media' by Hassanizadeh and Gray. *Transp. Porous Med.* **2**, 533–535 (1987). <https://doi.org/10.1007/BF00192153>
- Bear, J.: *Dynamics of Fluids in Porous Media*. Elsevier, New York (1972)
- Belhaj, H.A., Agha, K.R., Nouri, A.M., Butt, S.D., Vaziri, H.F. Islam M.R.: Numerical simulation of Non-Darcy flow utilizing the new Forchheimer's diffusivity equation. SPE 81499. In: Middle East Oil Show. Bahrain (2003). <https://doi.org/10.2118/81499-MS>
- Brown, K.E.: *The Technology of Artificial Lift Methods*, pp. 8–10. Petroleum Publishing Co., Tulsa (1980)
- Chilton, T.H., Colburn, A.P.: Pressure drop in packed tubes. *Ind. Eng. Chem.* **23**(8), 913–919 (1931). <https://doi.org/10.1021/ie50260a016>
- Choi, C.S., Song, J.J.: Estimation of the non-Darcy coefficient using supercritical CO₂ and various sandstones. *JCR Solid Earth.* **124**, 442–455 (2019). <https://doi.org/10.1029/2018JB016292>
- Coles, M.E., Hartman, K.J.: Non-Darcy measurements in dry core and the effect of immobile liquid. SPE 39977. In: SPE Gas Technology Symposium. Calgary (1998). <https://doi.org/10.2118/39977-MS>
- Cooper, J.W., Wang, X., Mohanty, K.K.: Non-Darcy flow studies in anisotropic porous media. *Soc. Petrol. Eng. J.* **4**(4), 334–341 (1999). <https://doi.org/10.2118/57755-PA>
- Cornell, D., Katz, D.L.: Flow of gases through consolidated porous media. *Ind. Eng. Chem.* **45**(10), 2145–2152 (1953). <https://doi.org/10.1021/ie50526a021>
- Darcy, H.P.G.: *Les Fontaines Publiques de la Ville de Dijon*. Victor Dalmont, Paris (1856)
- Ergun, S.: Fluid flow through packed columns. *Chem. Eng. Prog.* **48**(2), 89–94 (1952)
- Fancher, G.H., Lewis, J.A.: Flow of simple fluids through porous materials. *Ind. Eng. Chem.* **25**(10), 1139–1147 (1933). <https://doi.org/10.1021/ie50286a020>
- Firoozabadi, A., Katz, D.L.: An analysis of high-velocity gas flow through porous media. *J. Petrol. Technol.* (1979). <https://doi.org/10.2118/6827-PA>
- Firouzi, M., Alnoaimi, K., Kovscek, A., Wilcox, J.: Klinkenberg effect on predicting and measuring helium permeability in gas shales. *Int. J. Coal Geol.* **123**, 62–68 (2014). <https://doi.org/10.1016/j.coal.2013.09.006>
- Forchheimer, P.: Wasserbewegung durch Boden. *Z. Vereines deutscher Ing.* **45**(50), 1782–1788 (1901)
- Frederick, D.C., Grave, R.M.: New correlations to predict non-Darcy flow coefficients at immobile and mobile water saturation. SPE 28451. In: SPE Annual Technical Conference and Exhibition. New Orleans (1994). <https://doi.org/10.2118/28451-MS>
- Friedel, T., Voigt, H.D.: Investigation of non-Darcy flow in tight-gas reservoirs with fractured wells. *J. Pet. Sci. Eng.* **54**, 112–128 (2006). <https://doi.org/10.1016/j.petrol.2006.07.002>
- Fuente, M., Munoz, E., Sicilia, I., Goggins, J., Hung, L.C., Frutos, B., Foley, M.: Investigation of gas flow through soils and granular fill materials for the optimisation of radon soil depressurisation system. *J. Environ. Radioact.* **198**, 200–209 (2019). <https://doi.org/10.1016/j.jenvrad.2018.12.024>
- Geertsma, J.: Estimating the coefficient of inertial resistance in fluid flow through porous media. *Soc. Petrol. Eng. J.* (1974). <https://doi.org/10.2118/4706-PA>
- Ghane, E., Fausey, N.R., Brown, L.C.: Non-Darcy flow of water through woodchip media. *J. Hydrol.* **519**, 3400–3409 (2014). <https://doi.org/10.1016/j.jhydrol.2014.09.065>
- Gidley, J.L.: A method for correcting dimensionless fracture conductivity for non-Darcy flow effect. SPE 20710. SPE Prod. Eng. J. (1991). <https://doi.org/10.2118/20710-PA>
- Gjengedal, S., Brøtan, V., Buset, O.T., Larsen, E., Berg, O.A., Torsæter, O., Ramstad, R.K., Hilmo, B.O., Frengstad, B.S.: Fluid flow through 3D-printed particle beds: a new technique for understanding, validating, and improving predictability of permeability from empirical equations. *Transp. Porous Med.* **134**, 1–40 (2020). <https://doi.org/10.1007/s11242-020-01432-x>
- Green, L.J., Duwez, P.: Fluid flow through porous metals. *J. Appl. Mech.* **18**, 39–45 (1951)
- Holditch, S.A., Morse, R.A.: The effects of non-Darcy flow on the behavior of hydraulically fractured gas wells. *J. Pet. Technol.* **28**(10), 1179–1196 (1976). <https://doi.org/10.2118/5586-PA>

- Homuth, S., Götz, A.E., Sass, I.: Physical Properties of the geothermal carbonate reservoirs of the Molasse Basin, Germany-Outcrop Analogue vs. Reservoir Data. World Geothermal Congress, Melbourne (2015)
- Huang, H., Ayoub, J.A.: Applicability of the Forchheimer equation for non-Darcy flow in porous media. SPE 102715. In: SPE Annual Technical Conference and Exhibition. Texas (2008). <https://doi.org/10.2118/102715-MS>
- Hubbert, M.K.: Darcy law and the field equations of the flow of underground fluids. Trans. Am. Inst. Min. Metall. Eng. **207**, 222–239 (1956). <https://doi.org/10.2118/749-G>
- Irmay, S.: On the theoretical derivation of Darcy and Forchheimer formulas. J. Geophys. Res. **39**, 702–707 (1958). <https://doi.org/10.1029/TR039i004p00702>
- Janicek, J.D., Katz, D.L.: Applications of unsteady state gas flow calculations. In: Proceedings of University of Michigan Research Conference. June 20 (1955)
- Jones, S.C.: Using the inertial coefficient, β , to characterize heterogeneity in reservoir rock. SPE 16949. In: SPE Annual Technical Conference and Exhibition. New Orleans (1987). <https://doi.org/10.2118/16949-MS>
- Kadi, K.S.: Non-Darcy flow in dissolved gas-drive reservoirs. SPE 9301. In: SPE Annual Fall Technical Conference. Dallas (1980). <https://doi.org/10.2118/9301-MS>
- Klinkenberg, L.J.: The permeability of porous media to liquids and gases, drilling and production practice. Am. Petrol. Inst. 200–213 (1941)
- Kollbotn, L., Bratteli, F.: An alternative approach to the determination of the internal flow coefficient. In: International Symposium of the Society of Core Analysts. Toronto (2005)
- Kutasov, I.M.: Equation predicts non-Darcy flow coefficient. Oil Gas J. **91**(11), 66–67 (1993)
- Li, D., Engler, T.W.: Literature review on correlations of the non-Darcy coefficient. SPE 70015. In: SPE Permian Basin Oil and Gas Recovery Conference. Midland (2001). <https://doi.org/10.2118/70015-MS>
- Liu, X., Civan, F., Evans, R.D.: Correlation of the non-Darcy flow coefficient. J. Can. Pet. Tech. **34**(10), 50–54 (1995). <https://doi.org/10.2118/95-10-05>
- Ma, H., Ruth, D.W.: The microscopic analysis of high Forchheimer number flow in porous media. Transp. Porous Med. **13**, 139–160 (1993). <https://doi.org/10.1007/BF00654407>
- Macdonald, I.F., El-Sayed, M.S., Mow, K., Dullien, F.A.L.: Flow through porous media: the Ergun Equation revisited. Ind. Eng. Chem. Fundam. **18**, 189–208 (1979). <https://doi.org/10.1021/i160071a001>
- Macini, P., Mesini, E., Viola, R.: Laboratory measurements of non-Darcy flow coefficients in natural and artificial unconsolidated porous media. J. Pet. Sci. Eng. **77**(3–4), 365–374 (2011). <https://doi.org/10.1016/j.petrol.2011.04.016>
- Martins, J.P., Milton-Taylor, D., Leung, H.K.: The effects of non-Darcy flow in propped hydraulic fractures. SPE 20790. In: Proceedings of the SPE Annual Technical Conference. New Orleans (1990). <https://doi.org/10.2118/20709-MS>
- Mei, C.C., Auriault, J.L.: The effect of weak inertia on flow through a porous medium. J. Fluid Mech. **222**, 647–663 (1991). <https://doi.org/10.1017/S0022112091001258>
- Millionshikov, M.D.: Degeneration of homogeneous isotropic turbulence in a viscous incompressible fluid. Rep. Acad. Sci. USSR. **22**(5), 236–240 (1935) (in Russian)
- Morad, S., Al-Ramadan, K., Ketzer, J.M., De Ros, L.F.: The impact of diagenesis on the heterogeneity of sandstone reservoirs: a review of the role of depositional facies and sequence stratigraphy. AAPG Bull. **94**(8), 1267–1309 (2010). <https://doi.org/10.1306/04211009178>
- Muljadi, B.P., Blunt, M.J., Raeini, A.Q., Bijeljic, B.: The impact of porous media heterogeneity on non-Darcy flow behaviour from pore-scale simulation. Adv. Water. Resour. **95**, 329–340 (2016)
- Noman, R., Shrimanker, N., Archer, J.S.: Estimation of the coefficient of inertial resistance in high-rate gas wells. SPE 14207. In: SPE Annual Technical Conference. Las Vegas (1985). <https://doi.org/10.2118/14207-MS>
- Pavlovsky, N.: Theory of Movement of Groundwater Under Hydraulic Engineering Constructions and Its Main Applications. Publishing House of Science and Melioration Institute, Petrograd (1922) (in Russian)
- Rasolooarijaona, M., Auriault, J.L.: Nonlinear seepage flow through a rigid porous medium. Eur. J. Mech. B/ Fluids **13**, 177–195 (1994)
- Ruth, D., Ma, H.: On the derivation of the Forchheimer equation by means of the average theorem. Transp. Porous Med. **7**(3), 255–264 (1992). <https://doi.org/10.1007/BF01063962>
- Scheidegger, A.E.: The Physics of Flow Through Porous Media. University of Toronto Press, Toronto (1974)
- Shelkachev, V.N., Lapuk, B.B.: Groundwater Hydraulics. p. 736. ISBN: 5-93972-081-1, Moscow—Igevs (2001) (in Russian)

- Skjetne, E.: High-velocity flow in porous media; analytical, numerical and experimental studies. Doctoral Thesis at Department of Petroleum Engineering and Applied Geophysics, Faculty of Applied Earth Sciences and Metallurgy, Norwegian University of Science and Technology (1995)
- Skjetne, E., Auriault, J.L.: New insights on steady, non-linear flow in porous media. *Eur. J. Mech. B/Fluids* **18**(1), 131–145 (1999). [https://doi.org/10.1016/S0997-7546\(99\)80010-7](https://doi.org/10.1016/S0997-7546(99)80010-7)
- Tek, M.R., Coats, K.H., Katz, D.L.: The effect of turbulence on flow of natural gas through porous reservoirs. *J. Petrol. Technol. AIME Trans.* **222**, 799–806 (1962). <https://doi.org/10.2118/147-PA>
- Tessem, R.: High Velocity Coefficient's Dependence on Rock Properties: A Laboratory Study. Thesis Pet. Inst., NTH, Trondheim (1980)
- Thauvin, F., Mohanty, K.K.: Network modeling of non-Darcy flow through porous media. *Transp. Porous Media* **31**, 19–37 (1998). <https://doi.org/10.1023/A:1006558926606>
- Torsæter, O., Tessem, R., Berge, B.: High Velocity Coefficient's Dependence on Rock Properties. SINTEF report, NTH, Trondheim (1981)
- Whitaker, S.: The Forchheimer equation: a theoretical development. *Transp. Porous Media* **25**, 27–61 (1996). <https://doi.org/10.1007/BF00141261>
- Wodie, J.C., Levy, T.: Correction non lineaire de la loi de Darcy. *C. R. Acad. Sci.* **2**(312), 157–161 (1991)
- Wong, S.W.: Effect of liquid saturation on turbulence factors for gas-liquid systems. *J. Can. Petrol. Tech.* **9**(4), 274–278 (1970). <https://doi.org/10.2118/70-04-08>
- Wu, Y.S., Pruess, K., Persoff, P.: Gas flow in porous media with Klinkenberg effects. *Transp. Porous Media* **32**(1), 117–137 (1998). <https://doi.org/10.1023/A:1006535211684>
- Zeng, Z., Grigg, R.: A criterion for non-Darcy flow in porous media. *Transp. Porous Media* **63**, 57–69 (2006). <https://doi.org/10.1007/s11242-005-2720-3>
- Zolotukhin, A.B., Gayubov, A.T.: Machine learning in reservoir permeability prediction and modeling of fluid flow in porous media. *IOP Conf. Ser. Mater. Sci. Eng.* **700**, 012023 (2019). <https://doi.org/10.1088/1757-899X/700/1/012023>
- Zolotukhin, A.B., Ursin, J.R.: *Fundamentals of Petroleum Reservoir Engineering*. Høyskoleforlaget AS – Norwegian Academic Press, Kristiansand (2000b)
- Zolotukhin, A.B., Ursin, J.R.: *Introduction to Petroleum Reservoir Engineering*. Norwegian Academic Press, Høyskoleforlaget (2000a)

Publisher's Note Springer Nature remains neutral with regard to jurisdictional claims in published maps and institutional affiliations.